

Impact of Mobile Ions on Transient Capacitance Measurements of Perovskite Solar Cells

Moritz C. Schmidt¹, Emilio Gutierrez-Partida,² Martin Stolterfoht,^{2,3} and Bruno Ehrler^{1,*}

¹AMOLF, Science Park 104, 1098 XG, Amsterdam, The Netherlands

²Universität Potsdam, Am Neuen Palais 10, 14469 Potsdam, Germany

³The Chinese University of Hong Kong, Shatin, N.T., Hong Kong SAR



(Received 17 July 2023; revised 29 September 2023; accepted 17 October 2023; published 13 November 2023)

Mitigating the migration of mobile ions within perovskite solar cells is a crucial step on the way to improving their stability. In the past, transient capacitance measurements were applied to extract information about mobile ions, including their activation energy, diffusion coefficient, density, and polarity. However, in this work, we show that the interpretation of capacitance transients is more complex than originally proposed because of the intrinsic nature of the perovskite and the contributions of charge transport layers to the capacitance. Using drift-diffusion simulations and light-intensity-dependent capacitance transient measurements, we show that the direction of capacitance transients is not linked to the polarity of the migrating species. Instead, the direction of the transients is linked to the layer of the cell that dominates capacitance modulation. This work illustrates that transport layers can be crucial for the capacitance and impedance response of perovskite solar cells, and therefore, for characterizing mobile ions in perovskites.

DOI: 10.1103/PRXEnergy.2.043011

I. INTRODUCTION

Even though the efficiency of perovskite solar cells (PSCs) has increased significantly to 25.7% in 2023 [1], their commercialization is still hindered by their poor stability, which has been attributed to the migration of mobile ions in the perovskite layer [2]. Thus, to improve the stability of PSCs, significant efforts have been made to mitigate ion migration [3–5]. Based on calculations of defect formation energies, it has often been suggested that vacancy-mediated migration of iodide (I^-) and methylammonium (MA^+) contribute to ion migration in methylammonium lead triiodide ($MAPbI_3$), where iodide vacancies (V_I^+) generally show an activation energy around 0.25–0.4 eV lower than that of methylammonium vacancies (V_{MA}^-) [6–8]. Experimentally, a variety of characterization techniques have been applied to understand the formation and migration of mobile ions. Some of these techniques focus on qualitatively understanding which mobile ions are present in the perovskite. These techniques include time-of-flight secondary ion mass spectrometry [9,10], photothermal-induced resonance microscopy [11],

and Kelvin probe force microscopy [12]. Other techniques focus on quantifying the density of mobile ions, their activation energy, or diffusion coefficient. These include electrical measurements like impedance spectroscopy [13], bias-assisted charge extraction [2], and ionic conductivity measurements [14,15].

One popular technique that has been applied to quantify the density, diffusion coefficient, activation energy, and polarity of mobile ions is transient ion drift (TID) [16–20]. TID is closely related to impedance-based techniques and relies on measuring capacitance transients after an applied voltage pulse is released. The capacitance is modulated by mobile ions drifting within the perovskite layer, which allows the properties of these ions to be measured. The physical model behind TID is typically based on a few core assumptions, namely, that the perovskite has a high doping density, the ion density is much smaller than the doping density, and charge transport layers (CTLs) do not significantly contribute to the capacitance transients. Additionally, the direction of the capacitance transients was directly related to the polarity of ionic species, meaning that decreasing capacitance transients (for *p*-doped perovskites) were assigned to mobile anions (e.g., mobile I^- , Br_i^-), and increasing capacitance transients were assigned to mobile cations (e.g., mobile MA_i^+) [16,18].

Here, by utilizing drift-diffusion simulations of capacitance transients, we show that the interpretation of TID is more complex than originally expected. We show that

*b.ehrler@amolf.nl

Published by the American Physical Society under the terms of the [Creative Commons Attribution 4.0 International](#) license. Further distribution of this work must maintain attribution to the author(s) and the published article's title, journal citation, and DOI.

the direction of the transients is not related to the polarity of the ionic species. Instead, it depends on the layer in the device that dominates capacitance modulation by mobile ions. When the perovskite is fully depleted (low doping density), the accumulation of mobile ions at the perovskite-CTL interface leads to a depletion of electronic carriers in the CTLs, resulting in decreasing capacitance transients. In contrast, when the perovskite layer is only partially depleted, modulation of the depletion layer in the perovskite results in increasing capacitance transients. Between these regimes, the transients consist of a mixed regime, with an initial decrease, followed by an increase in capacitance. Lastly, we show experimentally that increasing the photogenerated carrier density of a PSC also leads to a change of the transient direction from decreasing to increasing, because of the change of the electric field distribution by photogenerated charges. Similar to doping, increasing the density of photogenerated carriers changes the layer that dominates capacitance modulation by mobile ions.

II. RESULTS AND DISCUSSION

To investigate the role of the polarity of mobile ions in capacitance measurements we simulate the behavior of the capacitance as a function of time after a voltage pulse. This simulation emulates the TID measurement. For the simulation of capacitance transients, we used the Setfos

drift-diffusion solver by FLUXiM. The device structure resembling a perovskite solar cell is shown in Fig. 1(c), and all simulation parameters are listed as parameter set 1 of Table S1 within the Supplemental Material [21]. For the CTLs, we selected parameters that were in the range of typical organic semiconductors used in PSCs (e.g., Poly[bis(4-phenyl)(2,4,6-trimethylphenyl)amine (PTAA) and C₆₀). However, to simplify the device structure, we used the same band gaps, effective density of states, mobilities of electronic carriers, and dielectric constants for both the hole transport layer (HTL) and electron transport layer (ETL). The simulation parameters for the perovskite layer are based on MAPbI₃. Throughout this work, we assume that two ionic species with opposite charges are present in the perovskite, where one species is mobile within the perovskite, while the other one is immobile and homogeneously distributed throughout the perovskite [22,23]. The densities of immobile and mobile ions are the same to ensure charge neutrality. We differentiate between positive ions and negative ions, where positive ions refer to positively charged interstitials and vacancies (e.g., iodide vacancies V_I⁺ and MA interstitials MA_i⁺), while negative ions refer to negatively charged interstitials and vacancies (e.g., iodide interstitials I_i⁻ and MA vacancies V_{MA}⁻). Additionally, we assume that the mobile ions are confined in the perovskite and cannot migrate into the CTLs.

Figure 1 shows a schematic of transient ion drift, considering positive mobile ions. Note that the device is

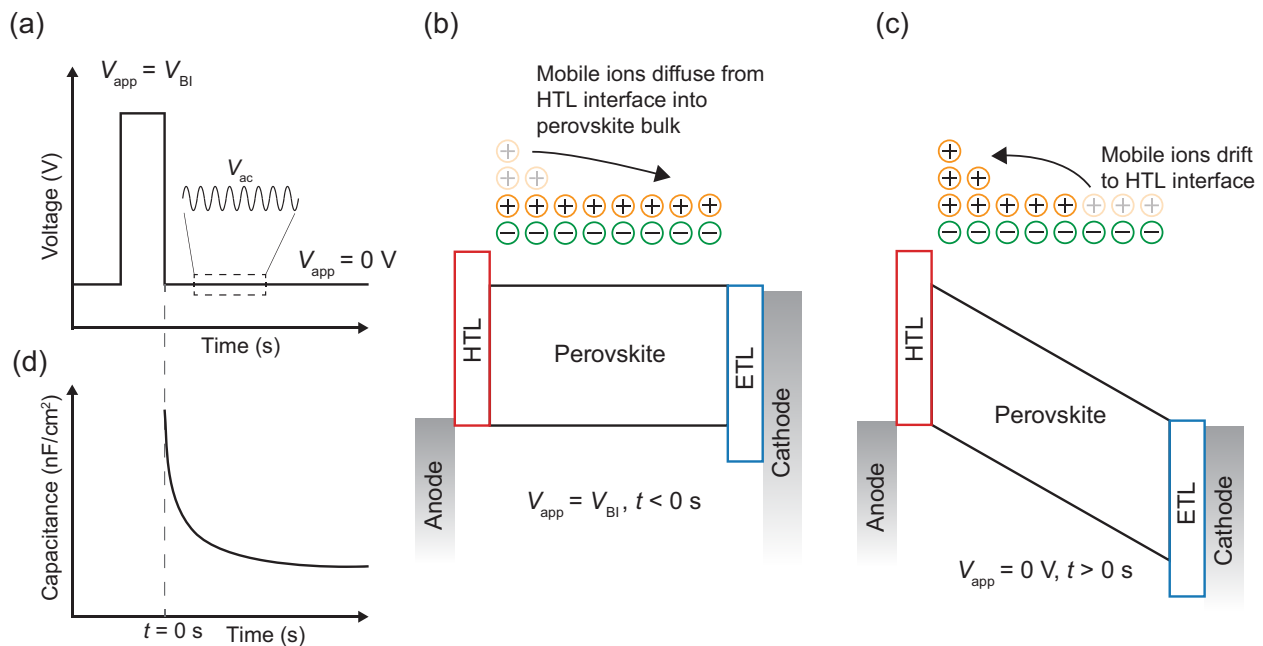


FIG. 1. (a) Illustration of the voltage profile applied to a perovskite solar cell during transient ion drift. After the voltage pulse, the capacitance of the device is probed with a high-frequency perturbation voltage, V_{ac} . (b) During the voltage pulse of $V_{app} = V_{BI}$, positive mobile ions that were previously accumulated at the HTL interface diffuse into the perovskite and are distributed more homogeneously. (c) When the voltage pulse is removed ($V_{app} = 0 \text{ V}$), positive mobile ions drift back to the HTL interface, changing the device capacitance. (d) Illustration of a capacitance transient.

symmetric, so, with negative mobile ions, we would see the same mechanism in the opposite direction. Initially, an external voltage equal to the built-in voltage, $V_{\text{app}} = V_{\text{BI}}$, is applied to the device [see Fig. 1(a)]. Because of compensation of the built-in field, mobile ions are distributed homogeneously within the perovskite [see Fig. 1(b)]. We note that, experimentally, the device might not reach this steady state if the voltage pulse is too short and some potential drops across the transport layers [24]. When the applied voltage is removed, $V_{\text{app}} = 0$ V, positive mobile ions drift to the perovskite-HTL interface to screen the built-in field [see Fig. 1(c)]. During the drift of ions, we simulate modulation of the capacitance using a perturbation voltage with a frequency of 10 kHz and an amplitude of 10 mV. At 10 kHz, the capacitance is determined by the density and distribution of electronic charge carriers within the PSC. Mobile ions do not directly contribute to the capacitance because they cannot follow the perturbed electric field due to their low mobility. However, they impact the distribution of electronic carriers within the PSC, and consequently, indirectly change the capacitance [25]. In other words, at the frequency of the perturbation, we are measuring a static distribution of ions, but over the timescale of milliseconds to seconds, the change in ion distribution changes the electronic capacitance of the device, resulting in a capacitance transient, as illustrated in Fig. 1(d).

We then use these simulations to better understand the transient capacitance measurements. First, we investigate how the polarity of the mobile ions influences capacitance transients. So far, in the literature, it has been assumed that the polarity of ionic charge carriers determines the direction of capacitance transients. This is analogous to the polarity of trap states in deep-level transient spectroscopy [26], which is very similar to TID. More specifically, decreasing transients were assigned to negative mobile ions like I_i^- or Br_i^- , while increasing transients were assigned to positive mobile ions like MA_i^+ [16,18] in a *p*-doped perovskite. The basis for this assignment was the assumption that the perovskite was doped, leading to a partially depleted perovskite, and the assumption that the density of mobile ionic carriers was smaller than the acceptorlike defect (or doping) density ($N_A > N_{\text{ion}}$). When applying a voltage pulse close to V_{BI} , the depletion layer would collapse and mobile ionic charge carriers would distribute homogeneously within the perovskite. After removing the applied voltage, mobile negative (positive) ions would drift out of the depletion layer, leading to an increase (decrease) in the depletion layer width. Because the depletion layer capacitance is proportional to the inverse of the depletion layer width, $C_{\text{DL}} \sim 1/w_{\text{DL}}$, this would ultimately result in increasing capacitance transients for negative ions and decreasing capacitance transients for positive ions [17]. Considering these conditions, we simulated capacitance transients for positive mobile and

negative ions, respectively. We chose an acceptor doping density of 10^{17} cm^{-3} and ionic carrier densities from 10^{15} to $5 \times 10^{16} \text{ cm}^{-3}$ (typical values for mobile ion densities extracted using TID lie between 10^{13} and 10^{16} cm^{-3} , while the assumed doping densities were around 1–2 orders of magnitude higher than the extracted ion densities [16,18–20]). The results are shown in Fig. 2, where $\delta C(t)$ is the capacitance change compared with the initial capacitance value, $\delta C(t) = C(t) - C_0$ (the transients of the absolute capacitance values are shown in Fig. S2 within the Supplemental Material [21]). As expected, the capacitance transients for mobile positive ions are increasing. However, contrary to the original prediction, the capacitance transients for negative mobile ions are also increasing. To better understand why both positive and negative mobile ions lead to increasing transients, we can study the energy band diagram and charge carrier distributions within the device. These are shown in Figs. 3(a)–3(c) for positive mobile ions. As expected, *p*-type doping of the perovskite leads to the formation of a depletion layer at the perovskite-ETL interface, where the depletion layer width [illustrated as w_0 in Fig. 3(c)] depends on the doping density and the density of ionic charge carriers in the depletion layer. Initially, when V_{BI} is applied to the device, mobile positive ions are distributed across the perovskite. Then, after removing V_{BI} , these mobile ions drift out of the depletion region towards the HTL [see Fig. 3(b)]. Because the acceptor atoms, N_A , and positive mobile ions have opposite polarity, the net charge density in the depletion layer increases. This, in turn, reduces the depletion layer width [to w_1 in Fig. 3(c)] and results in an increase in capacitance. In contrast, mobile negative ions accumulate at the perovskite-ETL interface after removing V_{BI} (see Fig. S3 within the Supplemental Material [21]). Now, the doping density and mobile negative ions have the same polarity. Consequently, the net charge density within the depletion layer increases upon the accumulation of mobile negative ions, leading to a decrease in the depletion layer width and an increase in capacitance. With this, we have established that the direction of capacitance transients cannot be correlated with the polarity of mobile ionic charge carriers. Instead, when considering high defect and doping densities, both negative and positive mobile ions lead to increasing capacitance transients. However, comparing the duration of the transients in Figs. 2(a) and 2(b), it is apparent that mobile negative ions lead to longer transients. These negative ions must partially diffuse through the field-free region of the perovskite before they accumulate in the depletion layer. In contrast, positive mobile ions only have to drift out of the depletion layer, leading to faster capacitance transients.

In the simulations shown so far, the capacitance transients were always increasing. However, decreasing or mixed transients are often observed in the literature, where mixed transients consist of an initial decrease

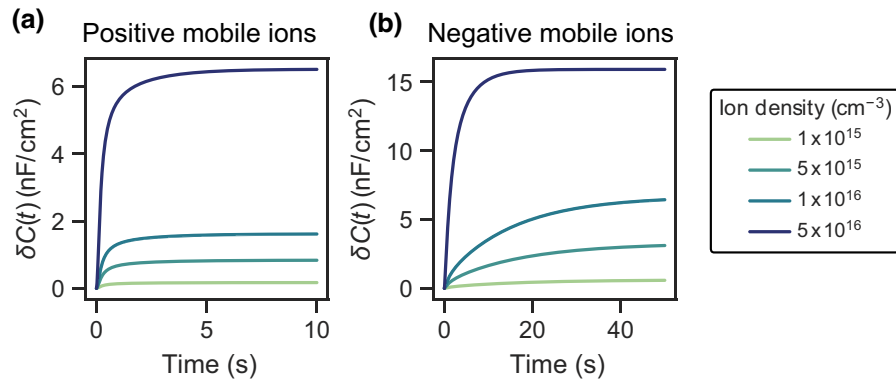


FIG. 2. Simulated capacitance transients for different ion densities in the case of (a) positive mobile ions and (b) mobile negative ions. In both cases, the acceptor doping density is 10^{17} cm^{-3} (*p*-type doping).

followed by an increase in capacitance [17–20]. Additionally, recent studies using intensity-dependent transient photoluminescence measurements, Hall measurements, and charge extraction by linearly increasing voltage measurements suggest that Pb-based PSCs are not significantly doped [27]. Therefore, we investigate the influence of doping density on capacitance transients next. Figure

4 shows the capacitance change of the decreasing and increasing components of simulated transients when considering acceptor doping densities between 5×10^{14} and $1 \times 10^{18} \text{ cm}^{-3}$, positive mobile ions resembling halide vacancies (as done similarly in Refs. [22,23,28]), and a mobile ion density of $5 \times 10^{16} \text{ cm}^{-3}$. Three different

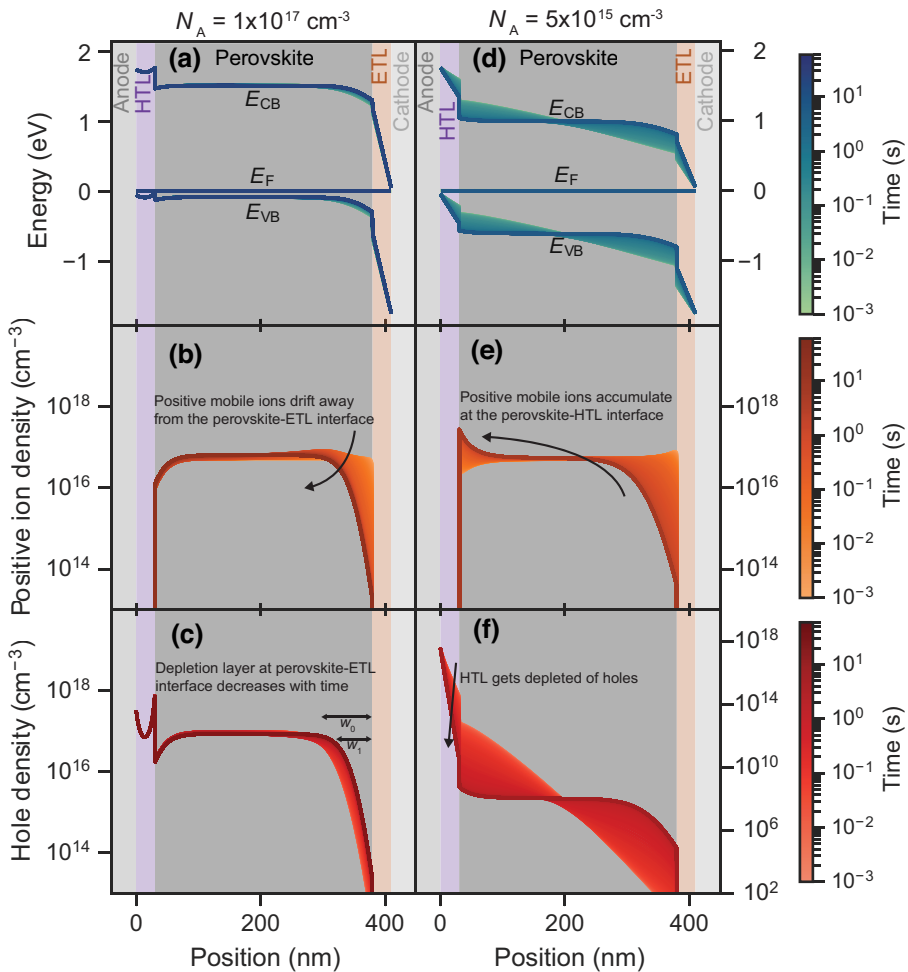


FIG. 3. Simulated energy band diagrams, positive mobile ion densities, and hole densities at different times during the transients. Ion density is $5 \times 10^{16} \text{ cm}^{-3}$. (a)–(c) Simulations in the case of an acceptor doping density of $1 \times 10^{17} \text{ cm}^{-3}$ (*p*-type doping). Corresponding increasing capacitance transient is shown in Figs. 2(a) and 4(c). (d)–(f) Simulations for an acceptor doping density of $5 \times 10^{15} \text{ cm}^{-3}$. Corresponding negative capacitance transient is shown in Fig. 4(a). Electron density distributions are shown in Fig. S6 within the Supplemental Material [21].

regimes are present (decreasing, mixed, and increasing), where one exemplary transient for each regime is shown in panels (a)–(c) (the transients with absolute capacitance values are shown in Fig. S4 within the Supplemental Material [21]). At doping densities up to around $2 \times 10^{16} \text{ cm}^{-3}$, the capacitance transients decrease. Then, up to $8 \times 10^{16} \text{ cm}^{-3}$ the transients consist of a decreasing and an increasing part. For doping densities above $8 \times 10^{16} \text{ cm}^{-3}$, the capacitance transients increase. We note that the same three regimes are also observed for mobile negative ions, as shown in Fig. S5 within the Supplemental Material [21]. This suggests that, rather than the polarity of mobile ionic species, the doping density of the perovskite determines the direction of capacitance transients.

We have already established that the increasing capacitance transients for high perovskite doping densities originate from a decrease in the depletion layer width in the perovskite when positive mobile ions drift out of the depletion layer. In contrast, in the case of low perovskite doping densities, the perovskite layer is depleted of electronic charge carriers, and its capacitance is given by the geometrical capacitance, $C_{\text{geo,pero}}$. Because $C_{\text{geo,pero}}$ is independent of the redistribution of ionic charge carriers, the perovskite layer does not contribute to the change of capacitance during the transient. Instead, the capacitance change originates from the transport layers. Upon application of the perturbation voltage, the density of charge carriers injected into the device changes and can be expressed as the capacitance:

$$C_\mu = \frac{dQ_{\text{inj}}}{dV_{\text{app}}} = e \frac{d}{dV} \int_0^d n(x) + p(x) dx, \quad (1)$$

where Q_{inj} is the injected charge; V_{app} is the applied voltage; e is the elementary charge; d is the thickness of the device; and $n(x)$ and $p(x)$ are the position-dependent electron and hole densities, respectively. This capacitance, C_μ , is sometimes termed chemical or charge storage capacitance [29,30]. A more detailed explanation of C_μ and the influence of mobile ions on it is given in Sec. S1 within the Supplemental Material [21]. Now, when positive mobile ions drift to the HTL-perovskite interface and accumulate there, the HTL gets more depleted of holes, as illustrated in Figs. 3(d)–3(f). At the same time, the depletion of positive ions at the perovskite-ETL interface leads to a reduction of electrons in the ETL [see Fig. S6(b) within the Supplemental Material [21]] because they are repelled by the net negative charge at the perovskite-ETL interface. The difference between the Fermi level and the valence band (VB) on the HTL side, and the Fermi level and the conduction band (CB) on the ETL side, increases [see Fig. 3(d)]. This results in a reduction of injected charge carriers upon application of the perturbed voltage, leading to a decrease of the capacitance, C_μ . We note that the injection of carriers into the perovskite could also contribute to C_μ . However, in the discussed case, the difference between the Fermi

level in the perovskite and its CB and VB is too large, and no significant density of electronic carriers is injected into the perovskite bulk. In the intermediate perovskite doping regime, the capacitance transients are mixed, consisting of an initial decrease followed by an increase in capacitance. After releasing the voltage pulse, positive mobile ions start accumulating at the HTL-perovskite interface, decreasing the density of holes in the HTL and in the perovskite close to the HTL (see Fig. S7 within the Supplemental Material [21]). This decrease, similar to the low doping case, results in the initial decrease in capacitance. Then, as more positive mobile ions accumulate at the HTL-perovskite interface, the built-in field is screened, resulting in a large portion of the perovskite being field free. In contrast to the low doping case, the energy difference between the Fermi level and the VB in the perovskite is smaller. Consequently, the injection of holes into the perovskite upon application of a perturbation voltage is significantly higher and increases as a larger fraction of the built-in field is screened. This ultimately results in the observed increase in capacitance.

Next to the doping density of the perovskite, other parameters of the PSC can impact the density of injected electronic carriers into the perovskite, and subsequently, C_μ and the increasing part of the transient. Because we assume the mobile ions to be positive, the injection of holes dominates C_μ of the perovskite. We, therefore, focus on the parameters of the HTL and the perovskite. We simulated the onset of the mixed transient regime, i.e., at which doping density the transients switch from decreasing to mixed (in Fig. 4, the onset would, for example, be at around a doping density of $2 \times 10^{16} \text{ cm}^{-3}$), as a function of ion density, thickness of the perovskite, VB offset between the HTL and perovskite, doping density of the HTL, and dielectric constant of the perovskite. The results are shown in Fig. S8 within the Supplemental Material [21]. Increasing the density of mobile ions within the perovskite shifts the onset of the mixed regime to slightly higher doping densities [see Fig. S8(a) within the Supplemental Material [21]]. This shift is strongly sublinear and can be explained in the following way: a higher ion density also leads to a higher density of accumulated positive ions at the HTL-perovskite interface. This results in a stronger depletion of holes at the HTL-perovskite interface, and consequently, reduces the overall density of injected holes in the perovskite, shifting the onset of the mixed regime to higher doping densities. When increasing the perovskite thickness, we observe that the onset of the mixed regime shifts almost linearly to lower doping densities because the built-in potential drops over an increasing distance [Fig. S8(b) within the Supplemental Material [21]]. For thicker films, a lower density of accumulated ions at the HTL-perovskite interface is necessary to screen the electric field. Consequently, more holes are injected into the perovskite, which results in a lower onset

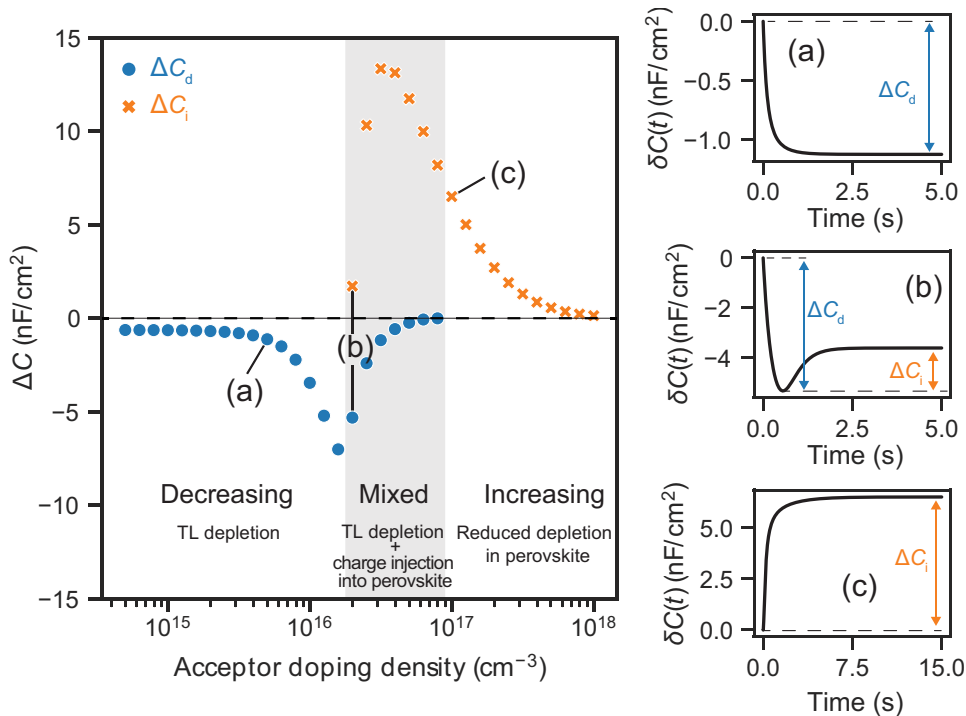


FIG. 4. Capacitance change, ΔC , of simulated capacitance transients, depending on the acceptor doping density of the perovskite. Simulated mobile ions are positive with a density of $5 \times 10^{16} \text{ cm}^{-3}$. ΔC is separated into decreasing transients (ΔC_d , blue circles) and increasing transients (ΔC_i , orange crosses). Depending on the acceptor doping density, three regimes are visible: decreasing (a), mixed (b), and increasing (c).

of the mixed regime. A higher dielectric constant of the perovskite results in a higher fraction of the potential dropping over the CTls. Consequently, the density of holes injected into the perovskite is reduced, shifting the onset of the mixed regime to higher doping densities [see Fig. S8(c) within the Supplemental Material [21]]. Changing the VB offset between the HTL and perovskite from -0.2 to 0.2 eV results in a stronger injection of holes into the perovskite. This leads to a shift of the onset of the mixed regime to lower doping densities [see Fig. S8(d) within the Supplemental Material [21]]. Lastly, increasing the doping density of the HTL leads to an increased injection of holes into the perovskite, shifting the onset of the mixed regime to dramatically lower doping densities [see Fig. S8(e) within the Supplemental Material [21]]. Here, at an HTL doping density of around $9 \times 10^{17} \text{ cm}^{-3}$, even undoped perovskites show a mixed transient, illustrating that injection of electronic carriers from the HTL into the perovskite effectively leads to an effectively doped perovskite layer.

In the previous section, we have established that the direction of capacitance transients depends on the layer that contributes to the capacitance. If the electronic carrier density of the perovskite is low, the CTls dominate the change in capacitance and the transients decrease. A sufficiently high electronic carrier density within the perovskite introduces an increasing

component. This increasing component can dominate the complete transient for significantly high doping in the perovskite. To verify these trends experimentally, we would ideally measure capacitance transients of PSCs with doping densities that span multiple orders of magnitude. However, accurate control of the doping density of perovskites is difficult to achieve [31]. Instead, we chose light excitation with a white high-power light-emitting diode (LED) to alter the electronic charge carrier density within the PSC. The PSC was based on the stack ITO/PTAA/PFN-P2/Cs_{0.05}(FA_{0.83}MA_{0.17})_{0.95}Pb(I_{0.84}Br_{0.16})₃/C₆₀/BCP/Cu, where PFN-P2 is Poly(9,9-bis(3'-(N,N-dimethyl)-N-ethylammonium-propyl-2,7-fluorene)-alt-2,7-(9,9-dioctylfluorene))dibromide, FA is Formamidinium, and BCP is Bathocuproine. The fabrication is described in the Supplemental Material [21]. These PSCs have been previously shown to have doping densities below 10^{13} cm^{-3} [32]. In addition, we use undoped organic CTls to ensure decreasing transients in the absence of light excitation. Exemplary $J-V$ curves at different light intensities, showing good diode character, are shown in Fig. S9 within the Supplemental Material [21]. In Fig. 5(a), the measured capacitance transients for different illumination intensities (from dark to 27.8 mW/cm^2) at 300 K are shown. We find that the transient direction switches with increasing light intensity. In the dark, the transient decreases throughout the entire time range. This is expected for a PSC

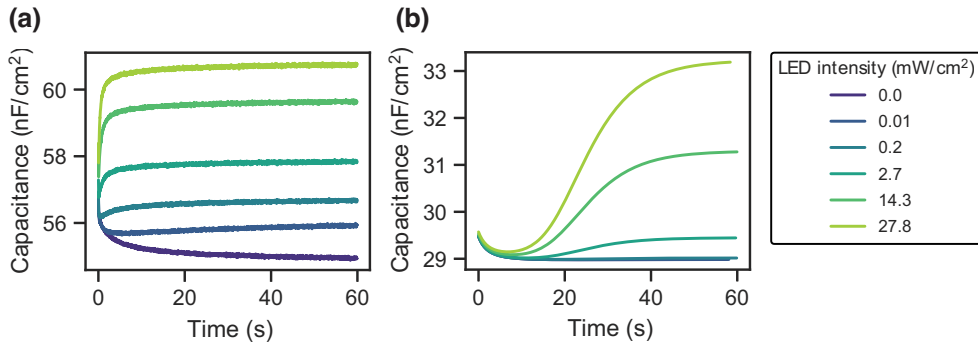


FIG. 5. (a) Measured capacitance transients of a perovskite solar cell at 300 K and different LED intensities. (b) Simulated capacitance transients of a perovskitelike semiconductor stack at different LED intensities, assuming $1 \times 10^{17} \text{ cm}^{-3}$ ions and positive mobile ions with a mobility of $3 \times 10^{-11} \text{ cm}^2/\text{Vs}$.

with a low doped perovskite. For low light intensities (e.g., 0.2 mW/cm^2), the transients show a decreasing and increasing component, where the magnitude of the increasing component strongly increases with light intensity. For the highest light intensity measured (27.8 mW/cm^2), we see a mostly increasing transient, with a small initial decrease remaining (see Fig. S10 within the Supplemental Material [21] for a magnification at short times). We additionally measured the capacitance transients at a range of different temperatures (172–330 K in steps of 8 K, see Fig. S11 within the Supplemental Material [21]). At lower temperatures, both components become slower, which means that at lower temperatures the decreasing transient becomes more obvious [see Fig. S11(d) within the Supplemental Material [21]]. On the contrary, the decreasing component vanishes completely from the measurement at high temperatures ($>318 \text{ K}$). This temperature dependence corresponds to the activation energy of the ionic processes, leading to the transients.

We qualitatively reproduce the light-intensity dependence of the measured capacitance transients using the drift-diffusion simulations described above and in the Supplemental Material [21]. The changes made to the model to approximate the device structure are listed as parameter set 2 in Table S1 within the Supplemental Material [21]. The results are shown in Fig. 5(b). We note that the simulations do not match the absolute capacitance values; this is most likely caused by differences in the doping density of the CTLs and dielectric constants of the CTLs and the perovskite. However, qualitatively, the simulations reproduce the trend that the capacitance transients transition from decreasing in the dark to mixed transients at higher light intensities. The light-induced splitting of the Fermi level and the subsequent decreasing difference to the CB and VB leads to an increase in C_μ of the perovskite. This is analogous to the case of higher doping, where an increase in the charge carrier density also leads to a contribution of the perovskite layer to the capacitance transient.

Interestingly, while the decreasing transient in the dark reproduces the time constant measured experimentally, the illuminated transients are much slower than the experimental data. A possible explanation for this discrepancy is that the mobility of mobile ions increases under illumination, as also found elsewhere [33,34]. This would result in faster transients, as illustrated in Fig. S12 within the Supplemental Material [21].

Finally, we note that the ionic contributions measured by the capacitance transients on these timescales (tens of seconds) are different from the ones typically measured by impedance spectroscopy and capacitance-frequency ($C\text{-}f$) methods. Because of low signal-to-noise ratios at low frequencies, $C\text{-}f$ spectra are usually measured to around 0.1 or 1 Hz, thus limiting the minimum resolvable mobility of ionic carriers. In contrast, capacitance transients can be measured for tens of seconds, allowing the characterization of mobile ionic carriers with a lower mobility compared to $C\text{-}f$. To illustrate this point, we measured the capacitance of our PSCs as a function of frequency, varying the temperature and light intensity. The results are shown in Fig. S13 within the Supplemental Material [21]. In the dark, we observe an increase in capacitance at around 1 kHz, which shifts to lower frequencies as the temperature decreases, in accordance with the literature [35]. We attribute this signature to mobile ions, the mobility of which decreases with decreasing temperature. We can qualitatively reproduce the $C\text{-}f$ measurements in simulations with ion mobilities of $1 \times 10^{-7} \text{ cm}^2/\text{Vs}$ at 332 K to $1 \times 10^{-10} \text{ cm}^2/\text{Vs}$ at around 200 K, as shown in Fig. S14 within the Supplemental Material [21]. Under illumination, the measurements and simulations are also in good agreement, as depicted in Figs. S13 and S14 within the Supplemental Material [21]. Here, we attribute the light-enhanced capacitance at low frequencies to phase-delayed recombination, as reported in the literature [36,37]. From the simulations, we can estimate the mobility of mobile ions at 300 K to be around $5 \times 10^{-8} \text{ cm}^2/\text{Vs}$. This value is much higher than the ionic mobility needed to reproduce the capacitance transients

in the dark ($\mu_{\text{ion}} = 3 \times 10^{-11} \text{ cm}^2/\text{Vs}$, see Fig. 5). This shows that the ionic response probed in the $C-f$ measurements is not the same as that observed at long times in the capacitance transients. Possibly, two mobile ionic species with very different mobilities are present in the perovskite, leading to dynamics on different timescales. This has similarly been proposed in Refs. [36,38,39] and shows the importance of both complementary methods. It also illustrates that a thorough investigation of the impact of multiple mobile ions with different ratios and mobilities on capacitance transients and $C-f$ measurements is necessary. We note, however, that accounting for multiple mobile ions with varying mobilities and densities significantly increases the parameter space for drift-diffusion simulations and is therefore beyond the scope of the work.

III. CONCLUSION

We have shown that the transient ion drift method, as applied in the literature so far, is more complex than originally proposed. An assignment of the polarity of mobile ions to the direction of capacitance transients is not possible. When, as assumed in the original transient ion drift model, the doping density of the perovskite is high, both positive mobile and negative ions result in an increase in the capacitance transient. When considering lower doping, the direction of the capacitance transient depends on whether the capacitance of the perovskite or CTLs is modulated when mobile ions drift through the perovskite. An accumulation of ions at the CTLs leads to a decrease in capacitance. Meanwhile, if the difference between the Fermi level and VB or CB is low enough, i.e., the perovskite is slightly doped, the chemical capacitance of the perovskite is modulated when mobile ions accumulate at the perovskite-CTL interfaces due to increased injection into the perovskite, leading to an increase in the overall capacitance. Experimentally, we have verified these findings by decreasing the difference between the Fermi level and VB or CB using illumination, which resulted in a change of the capacitance transients from decreasing to increasing. Finally, differences in time constants between $C-f$ measurements and transient ion drift measurements suggest that multiple ionic species are present in the PSC. Hence, our results show the breadth of timescales required to understand ion migration and perovskites, and that a greater understanding of these techniques by considering multiple mobile ionic species is needed.

ACKNOWLEDGMENTS

The authors thank Imme Schuringa for carefully reading and commenting on the manuscript. The work of M.C.S. and B.E. received funding from the European Research Council (ERC) under the European Union's Horizon 2020 research and innovation programme under Grant Agreement No. 947221. The work is part of the Dutch Research

Council and was performed at the AMOLF research institute. We acknowledge HyPerCells (a joint graduate school of the University of Potsdam and Helmholtz-Zentrum Berlin) and the Deutsche Forschungsgemeinschaft (DFG, German Research Foundation), Projects No. 423749265 and No. 424709669, SPP 2196 (SURPRISE-2 and HIPSTER-PRO) for funding. M.S. further acknowledges the Heisenberg program from the DFG, Project No. 498155101, and the CUHK Vice-Chancellor Early Career Professorship Scheme for funding.

M.C.S. conceived the work, carried out the simulations and experiments, performed the analysis, interpreted the results, and wrote the manuscript. B.E. conceived and supervised the work, interpreted the results, and edited the manuscript. E.G.P. fabricated the devices, and M.S. interpreted the transient capacitance results and edited the manuscript.

-
- [1] J. Park, J. Kim, H.-S. Yun, M. J. Paik, E. Noh, H. J. Mun, M. G. Kim, T. J. Shin, and S. I. Seok, Controlled growth of perovskite layers with volatile alkylammonium chlorides, *Nature* **616**, 724 (2023).
 - [2] J. Thiesbrummel, V. M. Le Corre, F. Peña-Camargo, L. Perdigón-Toro, F. Lang, F. Yang, M. Grischek, E. Gutierrez-Partida, J. Warby, M. D. Farrar, *et al.*, Universal current losses in perovskite solar cells due to mobile ions, *Adv. Energy Mater.* **11**, 2101447 (2021).
 - [3] E. Bi, Z. Song, C. Li, Z. Wu, and Y. Yan, Mitigating ion migration in perovskite solar cells, *Trends Chem.* **3**, 575 (2021).
 - [4] C. Kan, Z. Tang, Y. Yao, P. Hang, B. Li, Y. Wang, X. Sun, M. Lei, D. Yang, and X. Yu, Mitigating ion migration by polyethylene glycol-modified fullerene for perovskite solar cells with enhanced stability, *ACS Energy Lett.* **55**, 1 (2021).
 - [5] J.-W. Lee, S.-G. Kim, J.-M. Yang, Y. Yang, and N.-G. Park, Verification and mitigation of ion migration in perovskite solar cells, *APL Mater.* **7**, 041111 (2019).
 - [6] J. M. Azpiroz, E. Mosconi, J. Bisquert, and F. De Angelis, Defect migration in methylammonium lead iodide and its role in perovskite solar cell operation, *Energy Environ. Sci.* **8**, 2118 (2015).
 - [7] J. Haruyama, K. Sodeyama, L. Han, and Y. Tateyama, First-principles study of ion diffusion in perovskite solar cell sensitizers, *J. Am. Chem. Soc.* **137**, 10048 (2015).
 - [8] C. Eames, J. M. Frost, P. R. F. Barnes, B. C. O'Regan, A. Walsh, and M. S. Islam, Ionic transport in hybrid lead iodide perovskite solar cells, *Nat. Commun.* **6**, 7497 (2015).
 - [9] Z. Li, C. Xiao, Y. Yang, S. P. Harvey, D. H. Kim, J. A. Christians, M. Yang, P. Schulz, S. U. Nanayakkara, C.-S. Jiang, *et al.*, Extrinsic ion migration in perovskite solar cells, *Energy Environ. Sci.* **10**, 1234 (2017).
 - [10] D. Wei, F. Ma, R. Wang, S. Dou, P. Cui, H. Huang, J. Ji, E. Jia, X. Jia, S. Sajid, *et al.*, Ion-migration inhibition by the cation- π interaction in perovskite materials for efficient and stable perovskite solar cells, *Adv. Mater.* **30**, 1707583 (2018).

- [11] Y. Yuan, J. Chae, Y. Shao, Q. Wang, Z. Xiao, A. Centrone, and J. Huang, Photovoltaic switching mechanism in lateral structure hybrid perovskite solar cells, *Adv. Energy Mater.* **5**, 1500615 (2015).
- [12] J. S. Yun, J. Seidel, J. Kim, A. M. Soufiani, S. Huang, J. Lau, N. J. Jeon, S. I. Seok, M. A. Green, and A. Ho-Baillie, Critical role of grain boundaries for ion migration in formamidinium and methylammonium lead halide perovskite solar cells, *Adv. Energy Mater.* **6**, 1600330 (2016).
- [13] W. Peng, C. Aranda, O. M. Bakr, G. Garcia-Belmonte, J. Bisquert, and A. Guerrero, Quantification of ionic diffusion in lead halide perovskite single crystals, *ACS Energy Lett.* **3**, 1477 (2018).
- [14] D. Moia, J. Maier, and Ion Transport, Defect chemistry, and the device physics of hybrid perovskite solar cells, *ACS Energy Lett.* **6**, 1566 (2021).
- [15] G. Y. Kim, A. Senocrate, Y.-R. Wang, D. Moia, and J. Maier, Photo-effect on ion transport in mixed cation and halide perovskites and implications for photo-demixing, *Angew. Chem., Int. Ed.* **60**, 820 (2021).
- [16] M. H. Futscher, J. M. Lee, L. McGovern, L. A. Muscarella, T. Wang, M. I. Haider, A. Fakharuddin, L. Schmidt-Mende, and B. Ehrler, Quantification of ion migration in $\text{CH}_3\text{NH}_3\text{PbI}_3$ perovskite solar cells by transient capacitance measurements, *Mater. Horiz.* **6**, 1497 (2019).
- [17] M. H. Futscher, M. K. Gangishetty, D. N. Congreve, and B. Ehrler, Quantifying mobile ions and electronic defects in perovskite-based devices with temperature-dependent capacitance measurements: Frequency vs time domain, *J. Chem. Phys.* **152**, 044202 (2020).
- [18] L. McGovern, M. H. Futscher, L. A. Muscarella, and B. Ehrler, Understanding the stability of MAPbBr_3 versus MAPbI_3 : Suppression of methylammonium migration and reduction of halide migration, *J. Phys. Chem. Lett.* **11**, 7127 (2020).
- [19] L. McGovern, I. Koschany, G. Grimaldi, L. A. Muscarella, and B. Ehrler, Grain size influences activation energy and migration pathways in MAPbBr_3 perovskite solar cells, *J. Phys. Chem. Lett.* **12**, 2423 (2021).
- [20] S. Reichert, Q. An, Y.-W. Woo, A. Walsh, Y. Vaynzof, and C. Deibel, Probing the ionic defect landscape in halide perovskite solar cells, *Nat. Commun.* **11**, 6098 (2020).
- [21] See the Supplemental Material at <http://link.aps.org/supplemental/10.1103/PRXEnergy.2.043011> for details and parameters of the drift-diffusion simulations, experimental details, charge carrier density distribution and energy band diagrams during various transients, current density-voltage characteristics, additional capacitance transient measurements and simulations, and capacitance frequency measurements and simulations. It includes Refs. [24,29,38,40–50].
- [22] L. Bertoluzzi, C. C. Boyd, N. Rolston, J. Xu, R. Prasanna, B. C. O'Regan, and M. D. McGehee, Mobile ion concentration measurement and open-access band diagram simulation platform for halide perovskite solar cells, *Joule* **4**, 109 (2020).
- [23] G. Richardson, S. E. J. O'Kane, R. G. Niemann, T. A. Peltola, J. M. Foster, P. J. Cameron, and A. B. Walker, Can slow-moving ions explain hysteresis in the current–voltage curves of perovskite solar cells?, *Energy Environ. Sci.* **9**, 1476 (2016).
- [24] S. Ravishankar, Z. Liu, U. Rau, and T. Kirchartz, Multilayer capacitances: How selective contacts affect capacitance measurements of perovskite solar cells, *PRX Energy* **1**, 013003 (2022).
- [25] J. Diekmann, F. Peña-Camargo, N. Tokmoldin, J. Thiesbrummel, J. Warby, E. Gutierrez-Partida, S. Shah, D. Neher, and M. Stolterfoht, Determination of mobile ion densities in halide perovskites via low-frequency capacitance and charge extraction techniques, *J. Phys. Chem. Lett.* **14**, 4200 (2023).
- [26] D. V. Lang, Deep-level transient spectroscopy: A new method to characterize traps in semiconductors, *J. Appl. Phys.* **45**, 3023 (1974).
- [27] F. Peña-Camargo, J. Thiesbrummel, H. Hempel, A. Musienko, V. M. Le Corre, J. Diekmann, J. Warby, T. Unold, F. Lang, D. Neher, *et al.*, Revealing the doping density in perovskite solar cells and its impact on device performance, *Appl. Phys. Rev.* **9**, 021409 (2022).
- [28] N. E. Courtier, J. M. Cave, J. M. Foster, A. B. Walker, and G. Richardson, How transport layer properties affect perovskite solar cell performance: insights from a coupled charge transport/ion migration model, *Energy Environ. Sci.* **12**, 396 (2019).
- [29] J. Bisquert, Chemical capacitance of nanostructured semiconductors: its origin and significance for nanocomposite solar cells, *Phys. Chem. Chem. Phys.* **5**, 5360 (2003).
- [30] Chih-Tang Sah, The equivalent circuit model in solid-state electronics—part I: The single energy level defect centers, *Proc. IEEE* **55**, 654 (1967).
- [31] J. Euvrard, Y. Yan, and D. B. Mitzi, Electrical doping in halide perovskites, *Nat. Rev. Mater.* **6**, 531 (2021).
- [32] F. Peña-Camargo, M. Stolterfoht, H. Hempel, A. Musienko, V. M. Le Corre, J. Thiesbrummel, J. Warby, T. Unold, F. Lang, D. Neher, *et al.*, in *Proc. Int. Conf. Hybrid Org. Photovolt.* (Fundació Scito, 2022).
- [33] W. Zhou, Y. Zhao, X. Zhou, R. Fu, Q. Li, Y. Zhao, K. Liu, D. Yu, and Q. Zhao, Light-independent ionic transport in inorganic perovskite and ultrastable Cs-based perovskite solar cells, *J. Phys. Chem. Lett.* **8**, 4122 (2017).
- [34] J. Xing, Q. Wang, Q. Dong, Y. Yuan, Y. Fang, and J. Huang, Ultrafast ion migration in hybrid perovskite polycrystalline thin films under light and suppression in single crystals, *Phys. Chem. Chem. Phys.* **18**, 30484 (2016).
- [35] R. A. Awani, Z. Song, C. Chen, C. Li, C. Wang, M. A. Razooqi, L. Chen, X. Wang, R. J. Ellingson, J. V. Li, *et al.*, Influence of charge transport layers on capacitance measured in halide perovskite solar cells, *Joule* **4**, 644 (2020).
- [36] D. A. Jacobs, H. Shen, F. Pfeffer, J. Peng, T. P. White, F. J. Beck, and K. R. Catchpole, The two faces of capacitance: New interpretations for electrical impedance measurements of perovskite solar cells and their relation to hysteresis, *J. Appl. Phys.* **124**, 225702 (2018).
- [37] N. Filipoiu, A. T. Preda, D.-V. Anghel, R. Patru, R. E. Brophy, M. Kateb, C. Besleaga, A. G. Tomulescu, I. Pintilie, A. Manolescu, *et al.*, Capacitive and inductive effects in perovskite solar cells: The different roles of ionic current and

- ionic charge accumulation, *Phys. Rev. Appl.* **18**, 064087 (2022).
- [38] J. Thiesbrummel, S. Shah, E. Gutierrez-Partida, F. Zu, F. Camargo, S. Zeiske, J. Diekmann, F. Ye, K. Peters, K. Brinkmann, *et al.*, Ion induced field screening governs the early performance degradation of perovskite solar cells, (In Review, 2023).
- [39] D. Walter, A. Fell, Y. Wu, T. Duong, C. Barugkin, N. Wu, T. White, and K. Weber, Transient photovoltage in perovskite solar cells: Interaction of trap-mediated recombination and migration of multiple ionic species, *J. Phys. Chem. C* **122**, 11270 (2018).
- [40] N. Tessler and Y. Vaynzof, Insights from device modeling of perovskite solar cells, *ACS Energy Lett.* **5**, 1260 (2020).
- [41] M. Sendner, J. Trollmann, and A. Pucci, Dielectric function and degradation process of poly(triarylamine) (PTAA), *Org. Electron.* **15**, 2959 (2014).
- [42] M. Stolterfoht, P. Caprioglio, C. M. Wolff, J. A. Márquez, J. Nordmann, S. Zhang, D. Rothhardt, U. Hörmann, Y. Amir, A. Redinger, *et al.*, The impact of energy alignment and interfacial recombination on the internal and external open-circuit voltage of perovskite solar cells, *Energy Environ. Sci.* **12**, 2778 (2019).
- [43] Y. Ko, Y. Kim, C. Lee, Y. Kim, and Y. Jun, Investigation of hole-transporting poly(triarylamine) on aggregation and charge transport for hysteresisless scalable planar perovskite solar cells, *ACS Appl. Mater. Interfaces* **10**, 11633 (2018).
- [44] F. Staub, H. Hempel, J.-C. Hebig, J. Mock, U. W. Paetzold, U. Rau, T. Unold, and T. Kirchartz, Beyond bulk lifetimes: Insights into lead halide perovskite films from time-resolved photoluminescence, *Phys. Rev. Appl.* **6**, 044017 (2016).
- [45] F. Brivio, K. T. Butler, A. Walsh, and M. van Schilfgaarde, Relativistic quasiparticle self-consistent electronic structure of hybrid halide perovskite photovoltaic absorbers, *Phys. Rev. B* **89**, 155204 (2014).
- [46] M. Caputo, N. Cefarin, A. Radivo, N. Demitri, L. Gigli, J. R. Plaisier, M. Panighel, G. Di Santo, S. Moretti, A. Giglia, *et al.*, Electronic structure of MAPbI_3 and MAPbCl_3 : Importance of band alignment, *Sci. Rep.* **9**, 15159 (2019).
- [47] C. Q. Xia, J. Peng, S. Poncé, J. B. Patel, A. D. Wright, T. W. Crothers, M. Uller Rothmann, J. Borchert, R. L. Milot, H. Kraus, *et al.*, Limits to electrical mobility in lead-halide perovskite semiconductors, *J. Phys. Chem. Lett.* **12**, 3607 (2021).
- [48] C. Wehrenfennig, G. E. Eperon, M. B. Johnston, H. J. Snaith, and L. M. Herz, High charge carrier mobilities and lifetimes in organolead trihalide perovskites, *Adv. Mater.* **26**, 1584 (2014).
- [49] P. C. Eklund, A. M. Rao, Y. Wang, P. Zhou, K.-A. Wang, J. M. Holden, M. S. Dresselhaus, and G. Dresselhaus, Optical properties of C_{60} - and C_{70} -based solid films, *Thin Solid Films* **257**, 211 (1995).
- [50] C. H. Lee, G. Yu, D. Moses, V. I. Srdanov, X. Wei, and Z. V. Vardeny, Transient and steady-state photoconductivity of a solid C_{60} film, *Phys. Rev. B* **48**, 8506 (1993).